High-efficiency realization of the super-robust Rydberg Deutsch gate

A. Li [1], B.-B. Liu,[1] L.-L. Yan [1,2,*] S.-L. Su [1,2,†] Gang Chen,[1,‡] and M. Feng[3]

[1]*School of Physics and Laboratory of Zhongyuan Light, Zhengzhou University, Zhengzhou 450001, China*

[2]*Institute of Quantum Materials and Physics, Henan Academy of Sciences, Zhengzhou 450046, China*

[3]*State Key Laboratory of Magnetic Resonance and Atomic and Molecular Physics, Wuhan Institute of Physics and Mathematics, Innovation Academy of Precision Measurement Science and Technology, Chinese Academy of Sciences, Wuhan 430071, China*

(Received 4 September 2023; accepted 18 April 2024; published 3 June 2024)

Quantum logic gates are the essential components of quantum computation and have broad practical applications, especially for the multiple-qubit logic gates. Compared with appliying a series of single- and two-qubit gates, constrcuting quantum computation with multiple-qubit logic gates can be more efficient and high-fidelity. As a three-qubit logic gate, Deutsch gate enables the realization of any feasible quantum computations. Based on neutral atoms, we present a scheme of super-robust Deutsch gate via optimal control technique. Utilizing the Rydberg blockade effect of neutral atoms, we design an implementable D(β) based on the three-step program. One of the notable advantages of this function is that β can be achieved arbitrarily between 0 and π with the operation of target atom. In addition, we give an analytical solution agreed very well with numerical simulations for the residual blocking effect between next-neighbor atoms that affects the performance quality of Deutsch gate. The fidelity of our proposed scheme is demonstrated by numerical simulation of the master equation based on the full Hamiltonian, and the robustness of our scheme with control errors is also illustrated. Our proposal offers an alternative promising scheme for fault-tolerant quantum computation.

DOI: 10.1103/PhysRevResearch.6.023231

I. INTRODUCTION

Quantum computing has the potential superiority than classical computing in carrying out some certain computational tasks, such as the factorization of a large number via Shor's algorithm [1] and the search of an item in an unsorted database containing N elements [2]. To successfully execute quantum computation, an essential requirement is to construct a universal set of single- and two-qubit gates which own the high fidelity and strong robustness. However, a step-by-step combination scheme of single- and two-qubit gates [3–8] increases the complexity and the execution time of quantum computation, also wasting the quantum resources, since the number of operations grows polynomially with the increase of qubits. For example, if the Toffoli gate is implemented in this way, six CNOT and nine single-qubit quantum gates need to be combined [9,10]. To overcome these defects, the directly construct of multi-qubit logic gates in an efficient way has attracted extensive attention and has been achieved in a myriad of systems [11–15].

As one of the significant multiple-qubit gates, the Deutsch gate [16] makes the reliable large-scale quantum computing possible. Thus, it is significant to directly realize Deutsch gate. Directly realize the Deutsch gate via the dynamical protocol in neutral atoms system have been proposed [17]. However, the presence of the noise and operational errors during quantum system operations will inevitably limit the execute efficiency of the Deutsch gate [18]. Thus, how to construct the error-robust and high-fidelity Deutsch gate is a matter of concern.

Rydberg atoms, by exciting the neutral atoms to a large principal quantum number, have been applied in a variety of applications, because of their various excellent properties, e.g., strong and long-range interaction, long lifetime, and giant polarizability [19–21]. When excited to the Rydberg state, the Rydberg blockade effect [22–24] prevents the atoms from simultaneously transiting to the Rydberg state. Moreover, in light of the advancements made in trapping [25,26] and cooling [26,27] technologies, arrays of trapped neutral atoms interacting via the Rydberg blockade mechanism [28], have emerged as a potential scalable platform for quantum computing [28–35].

Quantum logic gates constructed by geometric phases [36–39] posses the intrinsic fault-tolerance feature, since the geometric phase only depends on the global geometric properties of the evolution path, instead of the specific evolution details. Nevertheless, the primitive geometric quantum computing scheme need to meet the adiabatic condition, which will reduce the gate speed, and thus amplify errors caused by environment-induced decoherence. To overcome this difficulty, nonadiabatic geometric quantum computation (NGQC) [40–46] and nonadiabatic holonomic quantum computation (NHQC) [47–59] based on the nonadiabatic Abelian and non-Abelian geometric phase [38,60] respectively have been

*llyan@zzu.edu.cn
†slsu@zzu.edu.cn
‡chengang971@163.com

proposed. Hereafter, there have been multifarious protocols proposed to further optimize the performance of the gate, such as the composite NHQC (CNHQC) scheme [61,62], the dynamical decoupling strategy [63,64], the deliberately optimal pulse-control technique [47,65–68], and path-shortening NHQC [69–73]. These schemes have been experimentally verified in a variety of physical platforms, such as superconducting circuits [74–77], nitrogen-vacancy (NV) center in diamond [78–80], and nuclear magnetic resonance (NMR) [81,82]. However, when considering the existence of system errors, these schemes do not meet our expectations, and their performance is not much improved compared to the dynamical schemes [42,57–59]. Here, we introduce a general NHQC proposal integrated with the dynamical-correction technique [83–85], termed as DCNHQC [68], which not only simplifies the gate operator but also meets the super-robust condition [86], i.e., the gate robustness against the control error can be improved from the second order to the fourth order.

In this manuscript, we propose a scheme to straightforwardly construct the Deutsch gate based on the Rydberg blockade mechanism, and combine the optimized pulses to further enhance the robustness against systematic errors. In order to have a better experimental choice, we consider to use the optimized pulses only on the target qubit or use optimized pulses on all three qubits to implement the Deutsch gate, and also compare them with the dynamical scheme [17]. As a result, our scheme constructs a Deutsch gate with high fidelity and strong fault tolerance for control errors involving geometric phases. Therefore our protocol provides a promising strategy for large-scale fault-tolerant quantum computation.

II. INTRODUCTION OF THE DEUTSCH GATE

A comprehensive description of this gate can be found in reference [17], hence we will provide a concise overview of the Deutsch gate. The Deutsch gate performs the following operation on the input state $|\psi_{\text{in}}\rangle = |a\rangle|b\rangle|c\rangle$,

$$|\psi_{\text{out}}\rangle = \begin{cases} i\cos\beta|a\rangle|b\rangle|c\rangle + \sin\beta|a\rangle|b\rangle|1-c\rangle, & a=b=1 \\ |a\rangle|b\rangle|c\rangle, & \text{otherwise} \end{cases}.$$

The parameter β can be varied within the interval $[0,\pi]$, representing a set of gates with different angles that enable the execution of various operations.

The angle-dependent nature makes it challenging to realize the Deutsch gate, there is a dynamical scheme proposed by Shi to achieve Deutsch's gate [17]. However, the experimental imperfect control will greatly affect the implementation performance of the gate. As proven in Sec. IV, this scheme can only suppress the driving field error to the second order, which is not experiment-friendly. In addition, it has been proven [87] that the realization of the Deutsch gate requires at least five two-qubit gates. However, the straightforward construction of a multiple-qubit logic gate greatly reduces the difficulty of gate operation and shortens the operation time. Therefore our focus is to propose a highly robust, straightforwardly implementable, and controllable β Deutsch gate scheme.

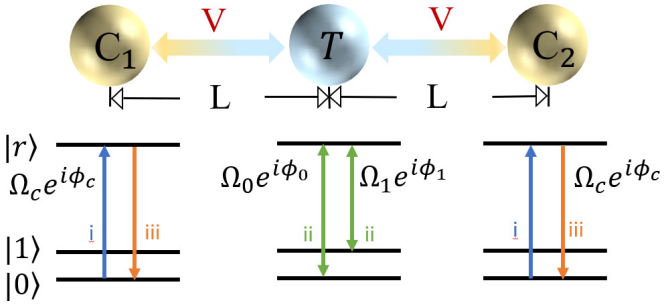

FIG. 1. The energy-level scheme to implement the super-robust Deutsch gate. The two outermost atoms are the control atoms C_1 and C_2 at the left and right, respectively, and the target atom in the middle is separated by a distance L, where an Rydberg interaction V arises when the target qubit and one of the two control qubits are in Rydberg state. The blue arrows, green arrows, and orange arrows represent the first to third steps in the implementation of a three-qubit super-robust Deutsch gate. For the control atoms, ground state $|0\rangle$ is resonantly coupled to Rydberg state $|r\rangle$ with the Rabi frequency $\Omega_c e^{i\phi_c}$. For target atom,ground states $|0\rangle$ and $|1\rangle$ are resonantly coupled to Rydberg state $|r\rangle$ with the Rabi frequency $\Omega_0 e^{i\phi_0}$ and $\Omega_1 e^{i\phi_1}$.

III. REALIZATION OF SUPER-ROBUST DEUTSCH GATE

A. A three-qubit Rydberg system

We consider a system composed of three Rydberg atoms, and the relevant configuration of the atomic level is illustrated in Fig. 1. The three Rydberg atoms are arranged in rows where the distance between two adjacent atoms is L. The two outermost atoms serve as control qubits, where target qubit is between them. The $|0\rangle$, $|1\rangle$ are the ground state and the $|r\rangle$ is the Rydberg state.

As shown in Fig. 1, the resonant laser with Rabi frequency $\Omega_c e^{i\phi_c}$ is implemented to couple the ground state $|0\rangle$ and Rydberg state $|r\rangle$ for control qubits, and the resonant laser with the Rabi frequency $\Omega_0 e^{i\phi_0}$ ($\Omega_1 e^{i\phi_1}$) is used to couple ground state $|0\rangle$ ($|1\rangle$) and Rydberg state $|r\rangle$ of target qubit. As both control qubits are in Rydberg state, there is a small interaction $V/2^6$ is induced. As one of the control qubits is excited in the state $|r\rangle$, the target qubit could not be excited to Rydberg state $|r\rangle$ due to the Rydberg-Rydberg interaction (RRI) with the strength $V = C_6/L^6$, where C_6 is the van der Waals interaction(vdWI) coefficient [88]. This blockade mechanism is the key to implement our protocols, which is modeled by the Hamiltonian $\hat{H}_{\text{V}} = \sum_{k=1}^{2} \text{V}|\text{rr}\rangle_{\text{ck,T}}\langle\text{rr}| + \text{V}/64|\text{rr}\rangle_{\text{c1,c2}}\langle\text{rr}|$, where the symbol 'ck' denotes the kth control atom, T denotes the target atom.

B. Super-robust Deutsch gate scheme

The super-robust Deutsch gate can be realized by following three steps.

Step (i). The resonant pulses are simultaneously applied on control atoms to make the transition from the ground-state $|0\rangle$ to Rydberg state $|r\rangle$ that is, $|0\rangle \mapsto i|r\rangle$, as shown in Fig. 2. As one of the control qubits in state $|0\rangle$ is excited to the Rydberg state $|r\rangle$ from the ground state, the Rydberg blockade effect makes target qubit stay in ground state. Considering different initial states, the following changes are observed:

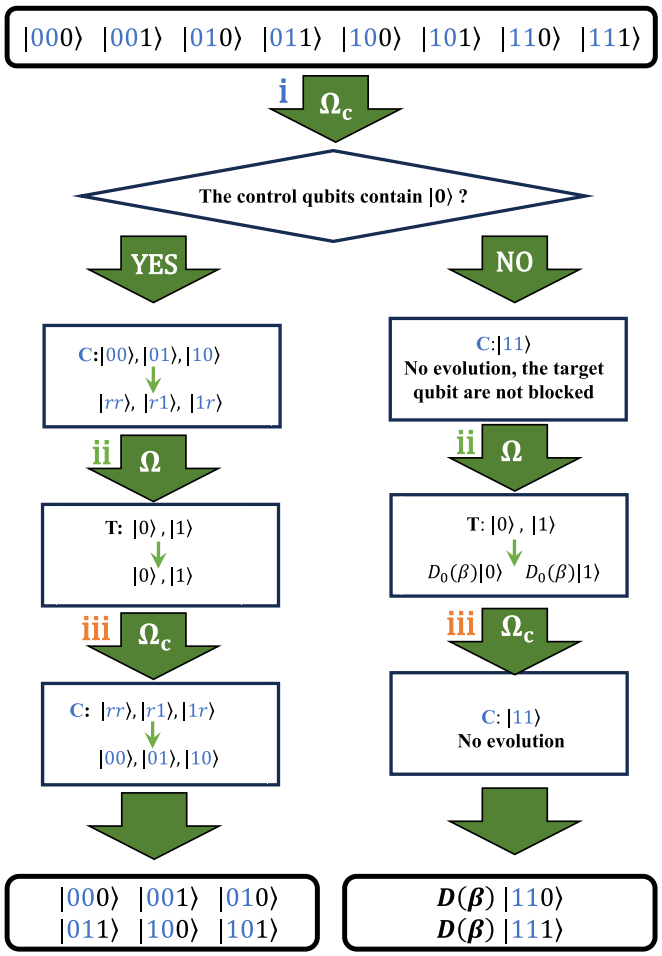

FIG. 2. Flow chart of constructing Deutsch gate,where C and T represent the control qubits (blue font) and target qubits (black font), respectively. The blue icon i, the green icon ii, and the orange icon iii, represent the pulse sequences (i.e., steps) of the whole process.

$\{|000\rangle, |001\rangle, |010\rangle, |011\rangle, |100\rangle, |101\rangle, |110\rangle, |111\rangle\} \mapsto -\{|rr0\rangle, |rr1\rangle, i|r10\rangle, i|r11\rangle, i|1r0\rangle, i|1r1\rangle, -|110\rangle, -|111\rangle\}$. In the rotating framework with respect to the driving frequency, assuming that the reduced Planck's constant $\hbar = 1$, the Hamiltonian of control atoms is

$$\hat{H}_{\rm C}^{1}(t) = \frac{1}{2}\Omega_c(t)e^{i\phi_c}\sum_{k=1}^{2}|0\rangle_{\rm ck}\langle r| + \text{H.c.}, \tag{1}$$

where $\int_0^{t_1}\Omega_c(t)dt = \pi$. When the control qubit is initialized in $|0\rangle$, the target qubit cannot be operated due to the RRI. Only both control qubits are in the $|1\rangle$ state, the target qubit can be implemented with desired operation.

Step (ii). The Hamiltonian of target atom can be expressed as

$$\hat{H}_{\rm T}(t) = \tfrac{1}{2}[\Omega_0(t)e^{i\phi_0(t)}|0\rangle + \Omega_1(t)e^{i\phi_1(t)}|1\rangle]\langle r| + \text{H.c.}, \tag{2}$$

where $\{|0\rangle, |1\rangle\}$ is computation basis, and $|r\rangle$ is the auxiliary state. Setting $\tan(\theta/2) = |\Omega_0(t)|/|\Omega_1(t)|$, we can get a set of time-independent orthogonal states $|b\rangle = \sin(\frac{\theta}{2})|0\rangle - \cos(\frac{\theta}{2})e^{i\phi}|1\rangle$, and a dark state of $|d\rangle = -\cos\frac{\theta}{2}e^{-i\phi}|0\rangle - \sin\frac{\theta}{2}|1\rangle$, which is decoupled from the other eigenstates during the quantum dynamical process. The Hamiltonian of the target atom can then be rewritten as

$$\hat{H}_{\rm T}(t) = \tfrac{1}{2}[\Omega(t)e^{i\phi_0(t)}|b\rangle\langle r|] + \text{H.c.}, \tag{3}$$

where $\phi_0 = \phi - \phi_1$, $\Omega(t) = \sqrt{\Omega_0(t)^2 + \Omega_1(t)^2}$. For a complete set of basis $\{|\psi_k(t)\rangle\}_{k=1}^{3}$ spanning a three-dimensional subspace, the time-dependent Schrodinger equation $i\frac{d}{dt}|\psi_k(t)\rangle = \hat{H}(t)|\psi_k(t)\rangle$ and the time evolution operator is $\hat{U}(t,0) = \hat{\mathcal{T}}e^{-i\int_0^t\hat{H}(t')dt'} = \sum_{k=1}^{3}|\psi_k(t)\rangle\langle\psi_k(0)|$, where $\hat{\mathcal{T}}$ denotes the time ordering operator. We require that the condition meets $-i\langle\psi_k(t)|\hat{H}_{\rm T}(t)|\psi_l(t)\rangle = 0$, that is, there is no accumulation of dynamical phase. After a complete cycle of evolution, the $|b\rangle$ state acquires a pure geometric phase γ_g, while state $|d\rangle$ stays unchanged. With the system errors to be considered, there may be undesired coupling between calculation subspaces and noncalculation subspaces, leading to a reduction fidelity of the solution. A solution is to impose the condition [86]

$$D_{km}(t) = \int_0^{\tau}\langle\psi_k(t)|\hat{H}(t)|\psi_m(t)\rangle dt = 0, \tag{4}$$

where $k = 1,\ 2,\ 3$ and $m = 1,\ 2$. To fulfill the condition, the evolution time τ_2 is partitioned into six segments. Specifically, the parameters must adhere to the following constrain:

$$\begin{aligned}
&\int_0^{\frac{\tau_2}{8}}\Omega(t)dt = \frac{\pi}{2}, \phi_0 = 0, \quad t\in\left[0,\frac{\tau_2}{8}\right],\\
&\int_{\frac{\tau_2}{8}}^{\frac{3\tau_2}{8}}\Omega(t)dt = \pi, \phi_0 = -\frac{\pi}{2}, \quad t\in\left[\frac{\tau_2}{8},\frac{3\tau_2}{8}\right],\\
&\int_{\frac{3\tau_2}{8}}^{\frac{\tau_2}{2}}\Omega(t)dt = \frac{\pi}{2}, \phi_0 = 0, \quad t\in\left[\frac{3\tau_2}{8},\frac{\tau_2}{2}\right],\\
&\int_{\frac{\tau_2}{2}}^{\frac{5\tau_2}{8}}\Omega(t)dt = \frac{\pi}{2}, \phi_0 = \gamma_g+\pi, \quad t\in\left[\frac{\tau_2}{2},\frac{5\tau_2}{8}\right],\\
&\int_{\frac{5\tau_2}{8}}^{\frac{7\tau_2}{8}}\Omega(t)dt = \pi, \phi_0 = \gamma_g+\frac{\pi}{2}, \quad t\in\left[\frac{5\tau_2}{8},\frac{7\tau_2}{8}\right],\\
&\int_{\frac{7\tau_2}{8}}^{\tau_2}\Omega(t)dt = \frac{\pi}{2}, \phi_0 = \gamma_g+\pi, \quad t\in\left[\frac{7\tau_2}{8},\tau_2\right].
\end{aligned} \tag{5}$$

At the end of the evolution, the evolution operator in the computational subspace can be obtained as $\hat{U}(\theta,\phi,\gamma_g) = e^{i\frac{\gamma_g}{2}}e^{-i\frac{\gamma_g}{2}\vec{\boldsymbol{n}}\cdot\vec{\boldsymbol{\sigma}}}$ with the vector $\vec{\boldsymbol{n}} = (\sin\theta\cos\phi, \sin\theta\sin\phi, \cos\theta)$ and Bloch vector $\vec{\boldsymbol{\sigma}} = (\sigma_x, \sigma_y, \sigma_z)$.

Step (iii). The orange arrows in Fig. 1 illustrate the de-excitation of two control qubits. A π pulse with a Rabi frequency Ω_c is applied to the two $|r\rangle$ states of the two control qubits, respectively. This pulse drives the control qubits from the Rydberg state$|r\rangle$ to the ground state $|0\rangle$. This process is governed by the Hamiltonian.

$$\hat{H}_{\rm C}^{2}(t) = -\frac{1}{2}\Omega_c(t)\sum_{k=1}^{2}|0\rangle_{\rm ck}\langle r| + \text{H.c.} \tag{6}$$

Then, by adjusting the values of parameters as $\phi = 0$, $\theta = \pi/2$, $\gamma_g = 2\beta$, one acquires the operation

$$\mathrm{D}(\beta) = \begin{pmatrix} \mathrm{I}_6 & 0 \\ 0 & \mathrm{D}_0(\beta) \end{pmatrix}, \tag{7}$$

where the core of the gate is defined by the matrix

$$\mathrm{D}_0(\beta) = \begin{pmatrix} i\cos\beta & \sin\beta \\ \sin\beta & i\cos\beta \end{pmatrix}, \tag{8}$$

where β is tunable in $[0, \pi]$. We can select different values of β to realize various gate operations. Currently, an optimized Deutsch gate operation has been successfully implemented. The total time to implement the enhanced-robustness Deutsch gate $D(\beta)$ is $T_1 = 2\pi/\Omega_c + 4\pi/\Omega$.

Subsequently, we endeavor to apply optimized pulses on the control qubits. Analogous to the operations performed on the target qubit, the control parameters must adhere to the following constraint:

$$\int_0^{3\tau_1} \frac{\dot{\beta}}{2} \exp\left(-i\int_0^t \frac{\dot{\phi_c}}{\cos\beta} dt'\right) dt = 0. \tag{9}$$

In order to meet this constraint, the parameters of the laser amplitude and phase satisfy the following relationships:

$$\begin{aligned}
&\int_0^{\tau_1} \Omega_c(t)dt = \pi, \phi_c = \pi/3, \qquad t \in [0, \tau_1], \\
&\int_{\tau_1}^{2\tau_1} \Omega_c(t)dt = \pi, \phi_c = -\pi/3, \qquad t \in [\tau_1, 2\tau_1], \\
&\int_{2\tau_1}^{\tau} \Omega_c(t)dt = \pi, \phi_c = \pi/3, \qquad t \in [2\tau_1, 3\tau_1],
\end{aligned} \tag{10}$$

where $\tau_1 = \pi/\Omega_c$. we have successfully achieved a highly robust population transition between the ground state $|0\rangle$ and the Rydberg state $|r\rangle$ of the control atoms. The total duration required to apply the optimized pulse on all three qubits is denoted as $T_2 = 6\pi/\Omega_c + 4\pi/\Omega$. Subsequently, we will demonstrate the performance of the Deutsch gate within our experimental framework.

IV. PERFORMANCE OF THE DEUTSCH GATE

We select $|r\rangle = |84p_{3/2}, m_j = 3/2\rangle$ for ^{133}Cs as the Rydberg state, the blockade mechanism has been experimentally demonstrated in [89], and the vdWI coefficient is obtained as $C_6/2\pi = -633$ GHz μm^6 [17,90–92]. The lifetime of the Rydberg state $|r\rangle$ is $\tau = 1.59$ ms under the temperature of 4.2 K [93], and the correspond decay rate is $\Gamma = 1/\tau = 0.6289$ KHz. Two ground states can be selected as $|0\rangle = |6s_{1/2}, F = 3, m_F = 0\rangle$ and $|1\rangle = |6s_{1/2}, F = 4, m_F = 0\rangle$ for the control and target qubits. The distance between these two identical Rydberg atoms is $L = 6$ μm, and the Rydberg interaction intensity is $V/2\pi = 13.57$ MHz.

To achieve perfect blocking, it is necessary to satisfy the conditions $|V|/64 \ll \Omega_c$ and $\Omega \ll |V|$, we select $\Omega_c/2\pi = 10$ MHz. In Fig. 3, examining the average fidelity variation of the optimized pulse applied solely to the target qubit against the optimized pulse applied to all three qubits, with the fluctuation of Ω, it is observed that the average fidelity of the super-robust Deutsch gate for both schemes exceeds

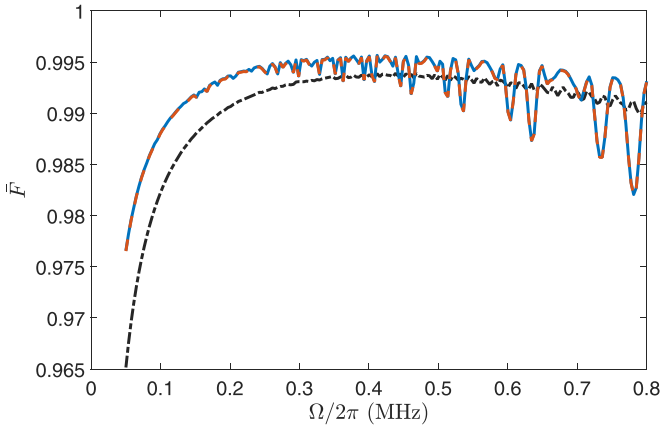

FIG. 3. The fidelities of different schemes to achieve the Deutsch gate under different laser Rabi frequency Ω, where the black dot-dashed curve, blue solid curve, and orange dash curve represent the results of dynamical scheme, the schemes of using the optimization pulses only on the target qubit, and on all three qubits, respectively. The fluctuation in fidelity of the super-robust scheme arises from the blocking leakage in the Rydberg system.

0.99 when $\Omega/2\pi$ ranges from 0.1216 to 0.6204 MHz. This phenomenon arises from the fact that if the Rabi frequency Ω is too small, the resulting longer evolution time increases susceptibility to decay errors, leading to a reduction in fidelity. On the contrary, if the Rabi frequency Ω is excessively large, the blocking conditions may not be effectively fulfilled. However, with respect to the next nearest neighbor atom, the blocking interaction $V/64$ impedes the transition between the control atoms and induces the phase accumulation, Consequently, this leads to an imperfect gate operation. (Further elaboration on this matter will be provided at the conclusion of this section). As depicted in Fig. 3, at a temperature of 4.2 K, the optimum fidelity achieved by applying the optimized pulse only on the target qubit is 0.99558. Meanwhile the optimum fidelity attained by applying the optimized pulse on all three qubits is 0.99552]corresponding to $\Omega/2\pi = 0.4246$ MHz, as utilized for numerical calculations in subsequent discussions.

Taking into account the impact of the decoherence, we conduct a numerical assessment of the gate performance using the Lindblad master equation

$$\dot{\hat{\rho}} = i[\hat{\rho}, \hat{H}(t)] + \frac{1}{2}\sum_{j=1}^{3}\sum_{i=0}^{2}(2\hat{L}_{ij}\hat{\rho}\hat{L}_{ij}^{\dagger} - \hat{L}_{ij}^{\dagger}\hat{L}_{ij}\hat{\rho} - \hat{\rho}\hat{L}_{ij}^{\dagger}\hat{L}_{ij}),$$

where $\hat{H}(t) = \hat{H}_{\mathrm{C}}^1(t) + \hat{H}_{\mathrm{C}}^2(t) + \hat{H}_{\mathrm{T}}(t) + \hat{H}_{\mathrm{V}}$ is the full Hamiltonian of the three-atom system, and $\hat{\rho}$ is the density operator. The atomic decay operator is defined by $\hat{L}_{ij} = \sqrt{\gamma_i}|i\rangle_j\langle r|$ with γ_i being the decay rates, and j labeling the jth atom. Furthermore, we introduce states $|2\rangle$ and $|2'\rangle$, with corresponding decay rates γ_2 and $\gamma_{2'}$, representing additional Zeeman sublevels apart from the quantum qubit states $|0\rangle$ and $|1\rangle$. For convenience, we assume that the decay rates from the Rydberg state $|r\rangle$ to the two ground states $|0\rangle$ and $|1\rangle$ are equal. As illustrated in Fig. 4(a), the leakage into the non-computational subspace is represented by the state $|2\rangle$. By scanning γ_2 from $0.1\gamma_0$ to $10\gamma_0$, where $\frac{\gamma_2}{\gamma_0} \in [0.1, 10]$, we have

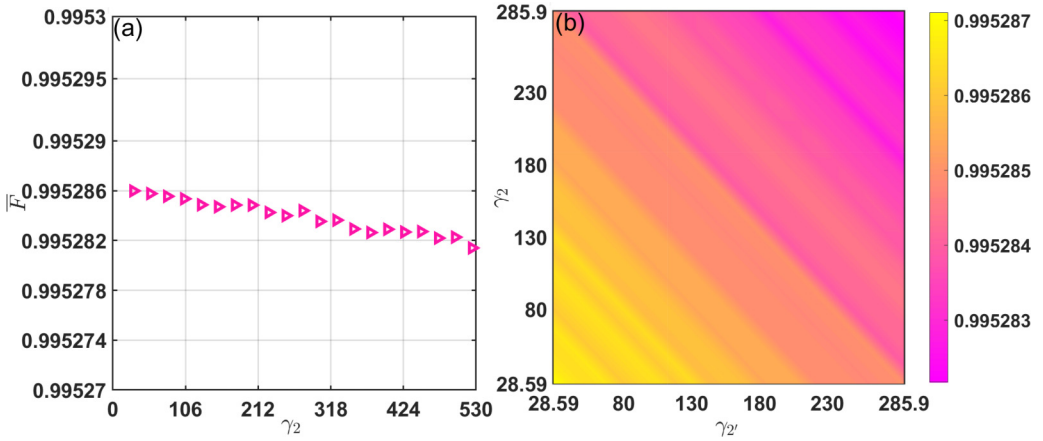

FIG. 4. The average fidelity variation of the Deutsch gates with the Rydberg states under different proportions leaking into computational and non computational subspaces (a).The parameter γ_2 is scanned from $0.1\gamma_0$ to $10\gamma_0$ to examine its influence on gate performance, (b). By scanning $\gamma_{2'} = \gamma_2$ from $0.1\gamma_0$ to $10\gamma_0$.

$\gamma_0 = \gamma_1 \in [\frac{\Gamma}{12}, \frac{10\Gamma}{21}]$ and $\gamma_2 \in [\frac{\Gamma}{21}, \frac{5\Gamma}{6}]$. It is observed that the fidelity remains approximately 0.9952. As depicted in Figure 4(b), the leakage into the noncomputational subspace is represented by the states $|2\rangle$ and $|2'\rangle$. Consequently, the decay rates have been reassigned such that $\gamma_0 = \gamma_1 \in [\frac{\Gamma}{22}, \frac{5\Gamma}{11}]$ and $\gamma_{2'} = \gamma_2 \in [\frac{\Gamma}{22}, \frac{5\Gamma}{11}]$, in contrast to the scenario where $\gamma_{2'} = \gamma_2 = 0$. Despite this adjustment, the fidelity exhibits only a slight change, from 0.9955 to 0.9952. To comprehensively assess the accuracy of the Deutsch gate, we employ the trace-preserving quantum-operator-based (TPQO) average fidelity comprehensively assess [94,95]

$$\overline{F}(\hat{U}_t, \hat{\xi}) = \frac{\sum_j tr(\hat{U}_t \hat{U}_j^\dagger \hat{U}_t^\dagger \hat{\xi}(\hat{U}_j)) + d^2}{d^2(d+1)}, \tag{11}$$

where $\hat{U}_j$ is the tensor of Pauli matrices, corresponding to $\hat{I}\hat{I}\hat{I}$, $\hat{I}\hat{I}\hat{\sigma}_x$, …, $\hat{\sigma}_z\hat{\sigma}_z\hat{\sigma}_y$, $\hat{\sigma}_z\hat{\sigma}_z\hat{\sigma}_z$. $\hat{U}_t$ is the ideal three-qubit Deustch gate, $d = 2^n$ with n denoting the numbers of qubit, and $\hat{\xi}$ is the trace preserving quantum operation.

Furthermore, the system will inevitably be affected by control errors. When considering the presence of these errors, the Hamiltonian of the system in Eqs. (2), (4), and (6) will change to

$$\begin{aligned}
\hat{H}_C^1(t) &= \left(\frac{1+\epsilon_1}{2}\right)\Omega_c(t)e^{i\phi_c}\sum_{k=1}^{2}|0\rangle_{ck}\langle r| + \text{H.c.},\\
\hat{H}_T(t) &= \left(\frac{1+\epsilon_2}{2}\right)\Omega(t)e^{i\phi_0(t)}|b\rangle\langle r| + \text{H.c.},\\
\hat{H}_C^2(t) &= \left(\frac{1+\epsilon_1}{2}\right)\Omega_c(t)e^{i\phi_c}\sum_{k=1}^{2}|0\rangle_{ck}\langle r| + \text{H.c.}
\end{aligned} \tag{12}$$

Here, we assume that the Rabi frequency fluctuation in the control and target qubits follow the same distribution for convenience, with both fluctuations ϵ_1 and ϵ_2 in the range of $-0.1 \leqslant \epsilon \leqslant 0.1$. As illustrated in Fig. 5(a), the super-robust schemes are more robust against the decay effect comparing with dynamical scheme due to their short evolution time. Initially, we examine the scenario without decay, depicted in Fig. 5(b), where we observe that when the error range is confined within 10%, the robustness of the optimized pulse is optimal across all three qubits. To further approximate real-world conditions, we conduct numerical simulations in the presence of decay, as illustrated in Fig. 5(c). In this scenario, if the Rabi error outweighs the decay error, employing the optimized pulse on all three qubits emerges as the optimal choice for implementing the super-robust Deutsch gate experimentally. Conversely, if the decay error is more significant, we recommend utilizing the optimization pulse

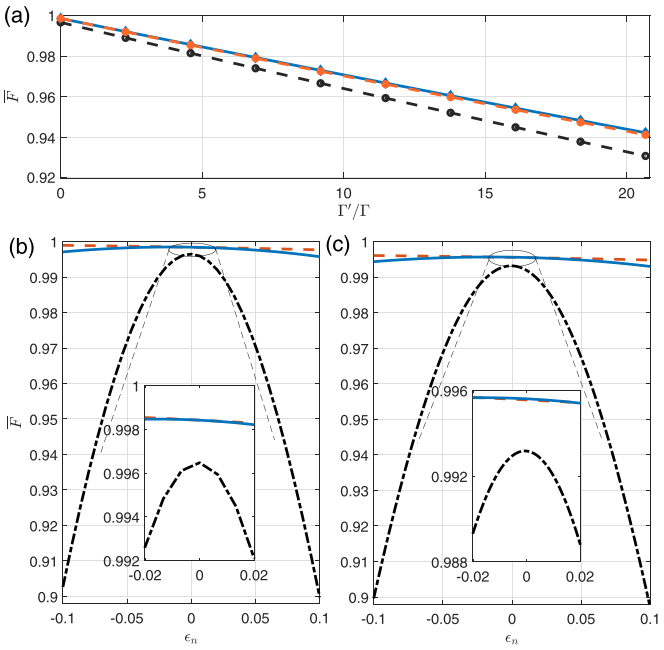

FIG. 5. The average fidelity of the three schemes fluctuates with (a) different decay rates Γ' (in unit of Γ), [(b) and (c)] the laser Rabi frequency fluctuations $\epsilon_n = \delta\Omega/\Omega \in [-0.1, 0.1]$, where (b) and (c) are corresponding to the cases without and with decay errors. The orange dashed curves, the solid blue curves and the black dot-dashed curves, represent the results of the schemes of using the optimization pulses on all three qubits and only on the target qubit, and dynamical scheme, respectively.

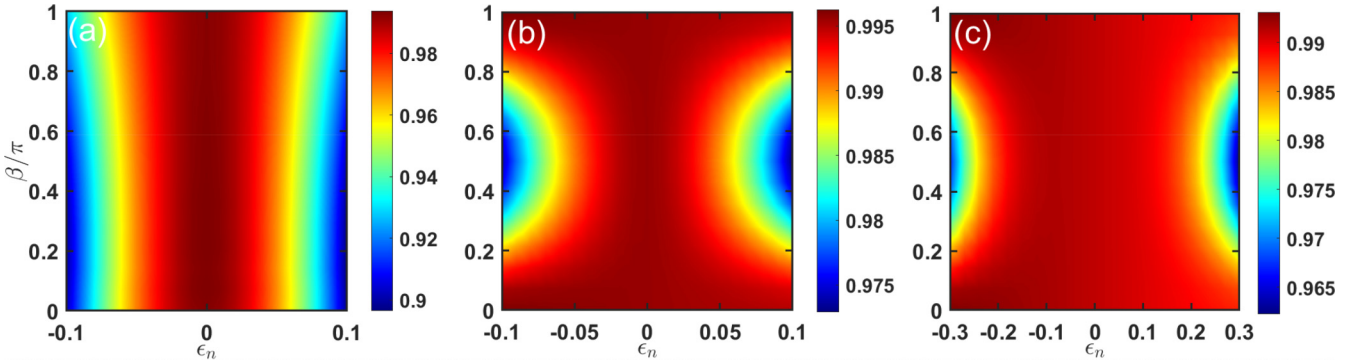

FIG. 6. Comparison of the fidelity of the Deutsch gate under the fluctuation of the Rabi frequency of the control and target qubits and the angle β under the regulation of 0 to π. (a) the dynamic scheme, (b) use the optimization pulse only on the target qubit, among them, we consider the control error fluctuation within 10%. (c) use the optimization pulse on all three qubits.

solely on the target qubit. For more quantitative comparison, we assume the fluctuation errors to obey the Gaussian distribution, i.e., $p(\epsilon) = \frac{1}{\sqrt{2\pi}\sigma} \exp(-\frac{\epsilon^2}{2\sigma^2})$ with σ representing the standard deviation of the exemplified errors. Based on the results, we thus obtain the fidelity of three protocols as 0.9932, 0.99558, and 0.99552, respectively, for the standard deviation $\sigma = 3\%$ of the Rabi frequency under the decoherence, while they are 0.9965, 0.9984, and 0.9984, respectively, without decoherence. Our scheme features an adjustable parameter β. Comparing the robustness against Rabi errors, Fig. 6 demonstrates that whether employing the optimization pulse solely on the target qubit or utilizing it on all three qubits, we can achieve a super-robust Deutsch gate with the β angle adjustable from 0 to π. In experiments, it is inevitable that the operations on the three pulses will suffer from errors originating from imprecise apparatus, imperfect control, so it is essential to investigate the effect of errors in timing control on the Deutsch gate performance. For the three-step pulse, we account for timing control errors t_f at two time points. t_{f1} considers the error at time t_1, while t_{f2} considers the error at time t_2 [96]. The scheme involves utilizing optimized pulses solely on the target qubit, with $t_1 = \pi/\Omega_c$ and $t_2 = \pi/\Omega_c + \tau_2$, and employing optimized pulse schemes on all three qubits, with the same time points t_1 and t_2. Here, $t_{f1,2} \in [-2.5, 2.5]$ ns. As depicted in Fig. 7(a) illustrates the scheme utilizing optimized

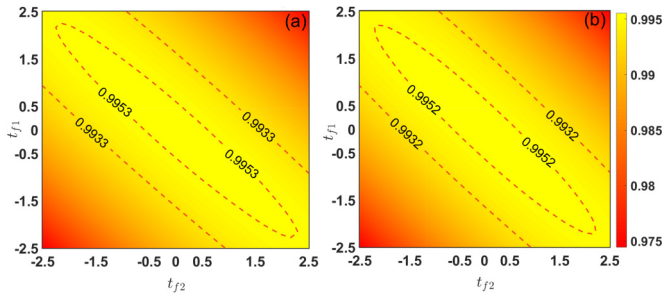

FIG. 7. The average fidelity of implementing super robust Deutsch gates under the errors in timing control, (a) the scheme of using optimized pulses only on the target qubit, at $t_1 = \pi/\Omega_c$ and $t_2 = \pi/\Omega_c + \tau_2$, (b) using optimized pulse schemes on all three qubits, at $t_1 = \pi/\Omega_c$ and $t_2 = \pi/\Omega_c + \tau_2$, where $t_{f1,2} \in [-2.5, 2.5]$ ns.

pulses solely on the target qubit, (b) represents the scheme employing optimized pulses on all three qubits. Consideration of $t_f = 1$ ns serves as an example: when two timing control points are either advanced or delayed by 1 ns simultaneously, the fidelity achieved using optimized pulses only on the target qubit is 0.9918, whereas the fidelity obtained using optimized pulse schemes simultaneously on three qubits is 0.9917. Consequently, it is observed that within the error range controlled by $t_f \in [-1, 1]$ ns, the fidelity of the super-robust Deutsch gate can still reach 0.99 or above. Conversely, when only two error symbols are opposite, the fidelity can also reach 0.99 or higher. Notably, if the excitation and de-excitation times of the control qubits are symmetrical, the impact on the fidelity of achieving the Deutsch gates can be disregarded.

The inability to cool atoms to absolute zero temperature within existing cooling mechanisms imposes limitations, as even at low temperatures, atomic motion induces the Doppler effect, causing motional dephasing during ground-Rydberg transitions. Some works have been made to mitigate Doppler dephasing errors in the implementation of Rydberg-mediated quantum gates [97–99]. We further calculate the infidelity resulting from the Doppler shift arising from thermal motion. Consequently, the Rabi frequencies for the Rydberg excitation are altered, $\Omega_c(t) \mapsto \Omega_c(t)e^{i\delta_1 t}$ $\Omega(t) \mapsto \Omega(t)e^{i\delta_2 t}$. The detunings $\delta_{1,2}$ of the excitation lasers experienced by the atoms are modeled as two random variables following a Gaussian probability distribution with a mean of $\delta_0 = 0$ and a standard deviation of $\sigma_\delta = k_w v$. Here, $k_w = 1.9723 \times 10^7 \mathrm{m}^{-1}$ denotes the magnitude of the wave vector, and $v = \sqrt{k_B T_a/m}$ represents the one-dimensional root-mean-square velocity of the atoms, where k_B is the Boltzmann constant, T_a is the atomic temperature, and m is the atomic mass. Observations indicate that when the temperature reaches 10 μK, the fidelity of the super-robust Deutsch gate decreases to 0.976 at $\Omega/2\pi = 5$ MHz. However, this error can be mitigated by trapping and cooling atoms at the onset of the gate sequence [97]. For instance, cooling atoms to their vibrational ground state can bring the quantum qubit closer to the trap center, thereby reducing errors [100,101]. Despite several μK being considered quite low, recent experimental advancements in Rydberg-gate setups have demonstrated the attainment of such temperatures [102,103]. In experimental contexts, Cs atomic systems have

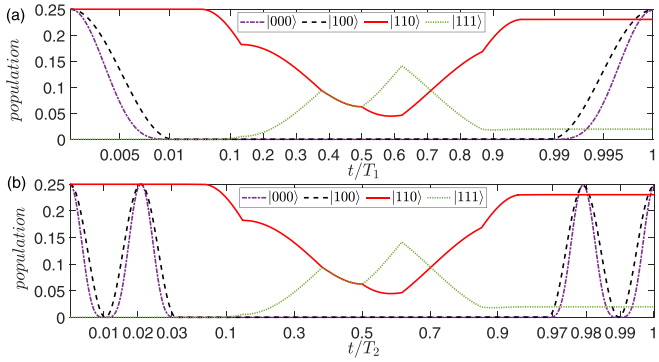

FIG. 8. The population dynamic of $|000\rangle$, $|100\rangle$, $|110\rangle$, $|111\rangle$ for the inital state $|\psi_0\rangle = (|000\rangle + |010\rangle + |110\rangle + |100\rangle)/2$. (a) and (b) represent the use of the optimization pulse on all three qubits, and only on the target qubit, respectively, where the extents of the control pulse segment are enlarged in the two sides of each figure. Set the β to arcsin $\frac{7}{25}$.

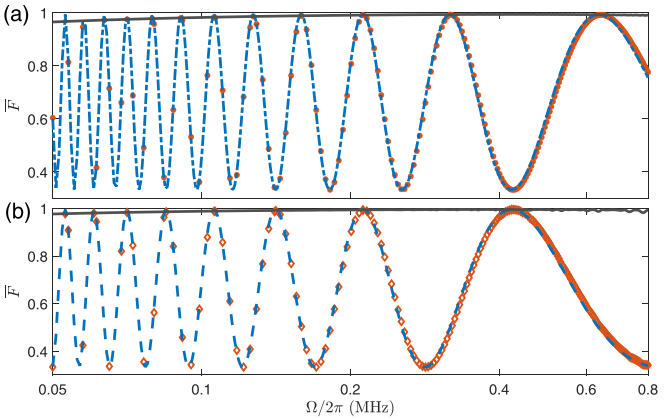

FIG. 9. The fidelity for the dynamical scheme (a) and the scheme using the optimization pulses only on the target qubit (b), where the red dot results are obtained by considering the influence of next nearest neighbor blocking interaction, i.e., $V/64$, the black solid curves are obtained without considering next nearest neighbor blocking interaction, and the blue dash curves denote the fitting curve obtained by the analytic formula $\overline{F} = A[1 + \cos(V\tau_2/64)]/2 + 1/3$ with A [=0.6598, 0.6619 for (a) and (b)] denoting the fitting coefficient.

reached temperatures as low as 4.2 μK. Even when maintaining a coupling strength of 3 MHz, the fidelity of the gate can still be upheld at 0.99.

The time-dependence of state populations is depicted in Fig. 8, initialized with the state $|\psi_0\rangle = (|000\rangle + |010\rangle + |110\rangle + |100\rangle)/2$. Figure 8(a) the scheme utilizing optimized pulses solely on the target qubit and Fig. 8(b) showcases the scheme employing optimized pulses on all three qubits. The absence of population changes in states $|110\rangle$ and $|111\rangle$ is attributed to both control atoms remaining unexcited to the Rydberg state by the control pulse. Additionally, during step (ii), the $|000\rangle$ and $|100\rangle$ states exhibit no distribution, stemming from the Rydberg blocking effect on the target atom induced by the Rydberg state excited by the control atom in step (i).

Finally, we consider the influence of next nearest neighbor blocking interaction, i.e., the effect of $V/64$, which induces a phase accumulation $\varphi = -\tau_2 V/64$ with τ_2 denoting the duration of controlling the target qubit. In dynamical scheme, $\tau_2 = 6\pi/\overline{\Omega}$ [17] and $\tau_2 = 4\pi/\Omega$ in our scheme. When $\varphi = (2N + 1)\pi$ with N being an integer, the obtained state will be orthogonal to the target state, resulting into zero fidelity. In these three schemes, there are two input states, i.e., $|000\rangle$ and $|001\rangle$ to be affected by the next nearest neighbor blocking interaction, thus, there will be 24 basis in the set constituted by $\{|000\rangle\langle 000|, |000\rangle\langle 001|, \ldots, |111\rangle\langle 111|\}$, will be affected, which contains one of $|000\rangle$, $|001\rangle$, $\langle 000|$ and $\langle 001|$. For the Pauli matrices $\hat{U}_j$ in Eq. (11), there will be 48 Pauli matrices affected by this effect. At $\varphi = (2N + 1)\pi$, the affected Pauli matrices gives no contribution to the average fidelity, resulting at only 1/4 of Pauli matrices set contributing to the average fidelity, which gives the average fidelity as

$$\overline{F} = (d^3/4 + d^2)/d^2(d + 1), \tag{13}$$

resulting $\overline{F} = 1/3$ for $d = 8$. Then, the average fidelity in our scheme can be obtained as

$$\overline{F} = A(1 + \cos(-\tau V/64))/2 + 1/3, \tag{14}$$

where the parameter A contains the error effects, such as operational error and decoherence. In the ideal condition, A equals to 2/3. These results can be demonstrated by Fig. 9, the details are given in Appendix A. To remove this unwanted phase accumulation, one method is to choose the parameters to make $\varphi = 2N\pi$, since $e^{2iN\pi} = 1$. In the foregoing discussion, we have use the relation $\overline{\Omega} = -3V/64$ and $\Omega = -V/32$ to make $\varphi = 2\pi$. The other method [17] is to choose three types of Rydberg states that are excited specifically from the first control qubit, the second control qubit, and the target qubit, respectively.

V. EXPERIMENTAL CONSIDERATIONS

A. Realization of the pulse

In experiments, two identical control atoms, confined within optical tweezers at a distance denoted by L, are subjected to an amplitude-modulated field with a Rabi frequency represented as $\Omega = \Omega e^{i\phi}$. This field is employed to induce transitions from the ground states $|0\rangle$ or $|b\rangle$ to the Rydberg state $|r\rangle$. The implementation of such amplitude modulation is achieved through the combined utilization of an acousto-optic modulator (AOM) and an arbitrary waveform generator, while the modulation of laser phase is also achievable through AOM modulation [104]. In addition, one of the primary challenges is to simultaneously use resonant light to excite two control atoms. This can be achieved by employing two laser beams with opposite k_w vectors to simultaneously illuminate the two atoms. To a certain extent, this approach can ensure precise alignment of the two laser beams onto the two atoms and maintain their relative phase stability. Since laser beams with opposite k_w vectors typically originate from opposite directions along the same optical path, they possess spatial symmetry, which helps mitigate alignment errors arising from path differences. In Fig. 10, we depict the profiles of phase and Rabi frequency, where (a) illustrates the scenario without optimized pulses on control qubits, while (b) portrays the case with optimized pulses on control qubits. It is evident that we

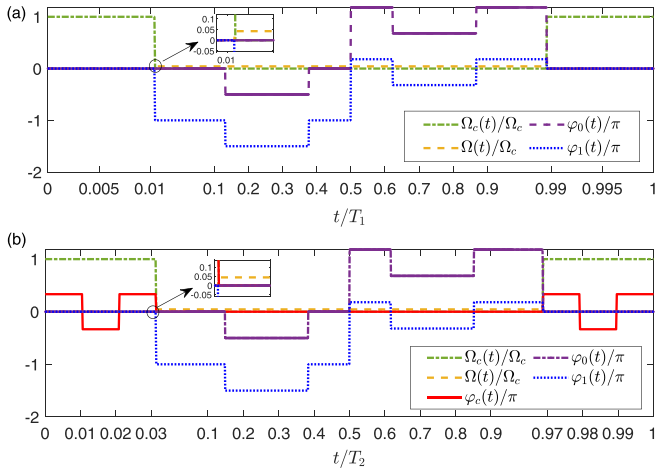

FIG. 10. Pulse diagram of our scheme. (a) is the scheme that use the optimized pulse only on the target qubit and (b) is the scheme that use the optimized pulse on all three qubits. The parameters are the same as those in Fig. 6.

exclusively modify the phase of the control pulse, leaving the Rabi frequency unchanged. This approach facilitates experimental manipulation.

B. Error analysis

A major contribution to the gate error is the decay of the Rydberg state, which can be minimized by using the higher Rydberg states and larger Ω_c values that, respectively, give lower decay rates and shorter gate times. The duration for each of the four input states to stay in Rydberg state is listed in Table I for the super-robust Deutsch gate protocol. The decay-induced fidelity error of the Deutsch gate averaged over the eight input states is $E_{\text{decay}} = \bar{T}_R/\tau$, where the $\bar{T}_{R_1} = T_{x_1} + \frac{4\pi-1}{16\Omega}$ is the time of the scheme using the optimization pulses only on the target qubit, $\bar{T}_{R_2} = T_{x_2} + \frac{4\pi-1}{16\Omega}$ is the scheme using the optimization pulses on the all three qubits.

Another fidelity error is the blockade error. During step (i) and step (iii), the input state $|000\rangle$ and $|001\rangle$ can not be fully converted back and forth to the state $|rr0\rangle$ and $|rr1\rangle$ because there is a residue blockade V/64 between the two control qubits when they are in Rydberg state. This contributes an error of about $E_b = 2(V/64)^2/\Omega_c^2$.

TABLE I. Time for the atoms to be in Rydberg states for different input states in the super-robust Deutsch gate protocol, where the $T_{x_1} = \pi/\Omega_c + 4\pi/\Omega$, $T_{x_2} = 3\pi/\Omega_c + 4\pi/\Omega$, the details are given in Appendix B.

Input state	T_{R_1}	T_{R_2}
$\|000\rangle$	$2T_{x_1}$	$2T_{x_2}$
$\|001\rangle$	$2T_{x_1}$	$2T_{x_2}$
$\|010\rangle$	T_{x_1}	T_{x_2}
$\|011\rangle$	T_{x_1}	T_{x_2}
$\|100\rangle$	T_{x_1}	T_{x_2}
$\|101\rangle$	T_{x_1}	T_{x_2}
$\|110\rangle$	$(4\pi-1)/(4\Omega)$	$(4\pi-1)/(4\Omega)$
$\|111\rangle$	$(4\pi-1)/(4\Omega)$	$(4\pi-1)/(4\Omega)$

C. Possible experimental configurations

With the development of quantum technology of Rydberg atoms trapped in optical lattices or tweezer arrays, a number of practical configurations of atomic arrays can be used to realize the proposed multiple-qubit gates if the Rydberg blockade condition is satisfied. Concretely, the one-dimensional [21,105,106] and two-dimensional [25,107] atomic array structures as well as the spherical structure can be considered for the experimental realization of the desired gate.

VI. CONCLUSION

In our approach, we leverage the Rydberg blockade effect alongside optimal control techniques and geometric quantum operations to straightforwardly realize a Deutsch gate with high fidelity and robustness. Furthermore, our protocol facilitates the implementation of Deutsch gates $\mathrm{D}(\beta)$ with arbitrary angles β, thus offering a comprehensive family of universal gates crucial for quantum computing [108]. Moreover, we carefully assessed the impact of control errors and decay errors on achieving high fidelity and robustness in our Deutsch gate implementation. When the decay error dominates over the Rabi error, we advocate for utilizing optimization pulses solely on the target qubit. Conversely, when the Rabi error prevails, employing optimization pulses on all three qubits is recommended. Comparative numerical simulations demonstrate the superior robustness of our scheme against both Rabi control errors and decay errors compared to previous proposals. Consequently, our proposal presents a promising avenue for advancing fault-tolerant quantum computation.

ACKNOWLEDGMENTS

This work is supported by the National Key R & D Program of China (Grants No. 2022YFA1404500, No. 2021YFA1400900), National Natural Science Foundation of China (Grants No. 12274376, No. 12074232, No. 12125406, No. 12074346, No. 12322410, No. U21A20434, No. 12204424, and No. 12147149), Cross-disciplinary Innovative Research Group Project of Henan Province (Grant No. 232300421004), Major science and technology project of Henan Province (Grant No. 221100210400) and Science Foundation for Excellent Young Scholars of Henan Province (Grants No. 232300421075 and No. 212300410085).

APPENDIX A: ANALYSIS FOR THE INFLUENCE OF THE NEXT NEAREST NEIGHBOR BLOCKING INTERACTION

In order to try to give an analytical solution for the subnearest neighbor interaction, we give the following analysis. In the basis space constituted by $\{|000\rangle\langle 000|, |000\rangle\langle 001|, \cdots, |111\rangle\langle 111|\}$, we rewrite them as $\hat{\sigma}_{n,l} = |n\rangle\langle l|$ with $n, l = s1, s2, \ldots, s8$ where we in order encode $s1 = 000$, $s2 = 001$, $s3 = 010$, $4 = 011$, $s5 = 100$, $s6 = 101$, $s7 = 110$, and $s8 = 111$. Due to $|000\rangle$ and $|001\rangle$ affected by the next nearest neighbor blocking interaction, an additional phase φ is produced in $|s1\rangle$ and $|s2\rangle$.

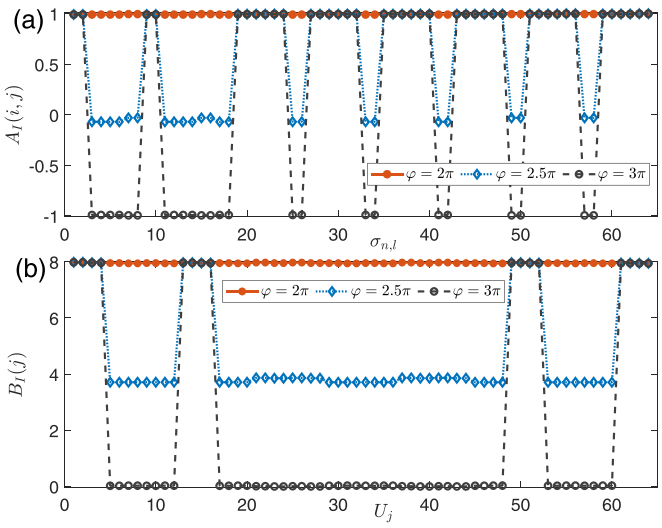

FIG. 11. The values for the fidelity of $\sigma_{n,l}$ (a) and U_j (b) for the basis sets $\{|000\rangle\langle 000|, |000\rangle\langle 001|, \ldots, |111\rangle\langle 111|\}$ and $\{\hat{I}\hat{I}\hat{I}, \hat{I}\hat{I}\hat{\sigma}_x, \ldots, \hat{\sigma}_z\hat{\sigma}_z\hat{\sigma}_y, \hat{\sigma}_z\hat{\sigma}_z\hat{\sigma}_z\}$, respectively, for different additional phase φ, under the scheme using the optimization pulses only on the target qubit.

Therefore, after an evolution superoperator $\hat{\xi}(\cdot)$ to produce a logic gate, the basis is changed into

$$\begin{aligned}
\hat{\sigma}^g_{n,l} &= e^{i\varphi}\hat{\xi}(\hat{\sigma}_{n,l}), \quad \text{if } n = s1, s2, l \neq s1, s2;\\
\hat{\sigma}^g_{n,l} &= e^{-i\varphi}\hat{\xi}(\hat{\sigma}_{n,l}), \quad \text{if } n \neq s1, s2, l = s1, s2;\\
\hat{\sigma}^g_{n,l} &= \hat{\xi}(\hat{\sigma}_{n,l}), \quad \text{others.}
\end{aligned} \tag{A1}$$

Then, the fidelity for these basis under the idea evolution U_{id} can be given as

$$\begin{aligned}
F_{n,l} &= e^{i\varphi}\mathrm{Tr}[\hat{\xi}(\hat{\sigma}_{n,l})\hat{U}_{id}\hat{\sigma}_{n,l}\hat{U}^\dagger_{id}], \quad \text{if } n = s1, s2, l \neq s1, s2;\\
F_{n,l} &= e^{-i\varphi}\mathrm{Tr}[\hat{\xi}(\hat{\sigma}_{n,l})\hat{U}_{id}\hat{\sigma}_{n,l}\hat{U}^\dagger_{id}], \quad \text{if } n \neq s1, s2, l = s1, s2;\\
F_{n,l} &= \mathrm{Tr}[\hat{\xi}(\hat{\sigma}_{n,l})\hat{U}_{id}\hat{\sigma}_{n,l}\hat{U}^\dagger_{id}], \quad \text{others,}
\end{aligned} \tag{A2}$$

where the phase induced by the next nearest neighbor blocking interaction has been distilled from the super-operator $\xi(\cdot)$. Thus the average fidelity of gate operator are given as

$$\overline{F} = \sum_{n,l=s1}^{s8} \frac{F_{n,l}}{64} = A_I\left[\frac{3}{8}(1+\cos\varphi) + \frac{1}{4}\right], \tag{A3}$$

where we have assume a constant coefficient $A_I = |A_I(n,l)| = \mathrm{Tr}[\hat{\xi}(\hat{\sigma}_{n,l})\hat{U}_{id}\hat{\sigma}_{n,l}\hat{U}^\dagger_{id}]$ for all $n, l = s1, s2, \ldots, s8$. Therefore there are only quarter of all the basis fully contributing to the average fidelity. As shown in Fig. 11(a), at the worst scenario $\cos\varphi = (2N+1)\pi$, there are 24 basis vectors that produce -1 effects and 40 that produce 1 effects, thus, the average fidelity is only $A_I/4$. If $\hat{\xi}(\hat{\sigma}_{n,l}) = \hat{U}_{id}\hat{\sigma}_{n,l}\hat{U}^\dagger_{id}$, $A_I = 1$, we have

$$\overline{F} = \tfrac{3}{8}(1+\cos\varphi) + \tfrac{1}{4}. \tag{A4}$$

At the worst scenario $\cos\varphi = (2N+1)\pi$, the average fidelity is only 0.25. These results are shown in Fig. 11(a), where the parameter $A_I \approx 0.99$. According to the above reasoning, changed into the basis set $\{\hat{I}\hat{I}\hat{I}, \hat{I}\hat{I}\hat{\sigma}_x, \ldots, \hat{\sigma}_z\hat{\sigma}_z\hat{\sigma}_y, \hat{\sigma}_z\hat{\sigma}_z\hat{\sigma}_z\}$, the average fidelity can be given phenomenology as

$$\overline{F} = \frac{\sum_j F_j + d^2}{d^2(d+1)} = \frac{d^2 B_I(3(1+\cos\varphi)/2+1)/4 + d^2}{d^2(d+1)}, \tag{A5}$$

where we assume the constant coefficient B_I for the contribution of F_j for $j = 1, 2, \ldots, 64$ by excluding the additional phasing. If $\hat{U}_t\hat{U}^\dagger_j\hat{U}^\dagger_t = \hat{\xi}(\hat{U}_j)$, $B_I = d$, which can be seen in Fig. 11(b) that $B_I = 7.95$ for $\varphi = 2\pi$. Therefore we can obtain

$$\overline{F} = \frac{3d(1+\cos\varphi)}{8(d+1)} + \frac{d+4}{4(d+1)}. \tag{A6}$$

Inserting $d = 8$, we can obtain

$$\overline{F} = \tfrac{1}{3}(2+\cos\varphi). \tag{A7}$$

If considering the dissipation and decoherence, a suitable fidelity formula can be written as $\overline{F} = A(1+\cos\varphi)/2 + 1/3$ with $A \approx 2/3$.

APPENDIX B: THE TIME FOR THE ATOM TO BE IN RYDBERG STATE

We have a detailed description of the time for the atoms to be in Rydberg states for different input states in the super-robust Deutsch gate protocol.

We first analyze the scheme used the optimized pulse only on the target qubit. For the case of no control atoms are excited to the Rydberg state, that is, the initial state is $|110\rangle$ or $|111\rangle$, where the target qubit is not blocked. Therefore we only need to consider the time of the target qubit on the Rydberg state,

$$\begin{aligned}
t_{r1} &= \int_0^{\frac{\pi}{2\Omega}} \frac{1}{2}\sin^2\frac{t\Omega}{2}dt = \frac{\pi-2}{8\Omega},\\
t_{r2} &= \int_{\frac{\pi}{2\Omega}}^{\frac{3\pi}{2\Omega}} \frac{1}{4}dt = \frac{\pi}{4\Omega},\\
t_{r3} &= \int_{\frac{3\pi}{2\Omega}}^{\frac{2\pi}{\Omega}} \frac{1}{4}(1+\sin t\Omega)dt = \frac{\pi-2}{8\Omega},\\
t_{r4} &= \int_{\frac{2\pi}{\Omega}}^{\frac{5\pi}{2\Omega}} \frac{1}{4}(1+\cos t\Omega)dt = \frac{\pi+2}{8\Omega},\\
t_{r5} &= \int_{\frac{5\pi}{2\Omega}}^{\frac{7\pi}{2\Omega}} \frac{1}{4}dt = \frac{\pi}{4\Omega},\\
t_{r6} &= \int_{\frac{7\pi}{2\Omega}}^{\frac{4\pi}{\Omega}} \frac{1}{4}dt = \frac{\pi}{8\Omega},
\end{aligned} \tag{B1}$$

the integrated population of the target qubit in $|r\rangle$ is

$$T_{R1} = \frac{2(\pi-2)}{8\Omega} + \frac{2\pi}{4\Omega} + \frac{\pi+2}{8\Omega} + \frac{\pi}{8\Omega} = \frac{4\pi-1}{4\Omega}. \tag{B2}$$

For the case of only one control atom is excited to Rydberg state, that is, the initial state is $|010\rangle$, $|011\rangle$, $|100\rangle$, or $|101\rangle$, the time for the atoms to be in Rydberg states is

$$T_{R1} = \int_0^{\frac{\pi}{\Omega_c}} \sin\frac{t\Omega_c}{2}dt + \tau_2 + \int_{\frac{\pi}{\Omega_c}}^{\frac{2\pi}{\Omega_c}} \cos\frac{t\Omega_c}{2}dt = T_{x1}. \tag{B3}$$

For both control atoms are excited to the Rydberg state, that is, the initial state is $|000\rangle$ or $|001\rangle$

$$T_{R1} = 2T_{x1}. \tag{B4}$$

Therefore the total decay error is

$$E_{\text{decay}} = \bar{T}_{R_1}/\tau, \tag{B5}$$

where

$$\bar{T}_{R_1} = T_{x_1} + \frac{8\pi - 2}{32\Omega}, \tag{B6}$$

Similarly, the scheme used optimized pulses on all three qubits is similar to the above calculation.

[1] P. W. Shor, Algorithms for quantum computation: discrete logarithms and factoring, in *Proceedings 35th Annual Symposium on Foundations of Computer Science* (IEEE Computer Society Press, Washington, DC, USA, 1994), pp. 124–134.

[2] L. K. Grover, Quantum mechanics helps in searching for a needle in a haystack, Phys. Rev. Lett. **79**, 325 (1997).

[3] D. Møller, L. B. Madsen, and K. Mølmer, Quantum gates and multiparticle entanglement by Rydberg excitation blockade and adiabatic passage, Phys. Rev. Lett. **100**, 170504 (2008).

[4] E. Urban, T. A. Johnson, T. Henage, L. Isenhower, D. D. Yavuz, T. G. Walker, and M. Saffman, Observation of Rydberg blockade between two atoms, Nat. Phys. **5**, 110 (2009).

[5] A. Barenco, C. H. Bennett, R. Cleve, D. P. DiVincenzo, N. Margolus, P. Shor, T. Sleator, J. A. Smolin, and H. Weinfurter, Elementary gates for quantum computation, Phys. Rev. A **52**, 3457 (1995).

[6] M. Saffman and K. Mølmer, Efficient multiparticle entanglement via asymmetric Rydberg blockade, Phys. Rev. Lett. **102**, 240502 (2009).

[7] S.-B. Zheng, Implementation of Toffoli gates with a single asymmetric Heisenberg XY interaction, Phys. Rev. A **87**, 042318 (2013).

[8] M. A. Nielsen, I. Chuang, and L. K. Grover, Quantum computation and quantum information, Am. J. Phys. **70**, 558 (2002).

[9] V. V. Shende and I. L. Markov, On the cnot-cost of TOFFOLI gates, Quantum Inf. Comput. **9**, 461 (2009).

[10] L. Henriet, L. Beguin, A. Signoles, T. Lahaye, A. Browaeys, G.-O. Reymond, and C. Jurczak, Quantum computing with neutral atoms, Quantum **4**, 327 (2020).

[11] M. Khazali and K. Mølmer, Fast multiqubit gates by adiabatic evolution in interacting excited-state manifolds of Rydberg atoms and superconducting circuits, Phys. Rev. X **10**, 021054 (2020).

[12] M. Li, F.-Q. Guo, Z. Jin, L.-L. Yan, E.-J. Liang, and S.-L. Su, Multiple-qubit controlled unitary quantum gate for Rydberg atoms using shortcut to adiabaticity and optimized geometric quantum operations, Phys. Rev. A **103**, 062607 (2021).

[13] L. Isenhower, M. Saffman, and K. Mølmer, Multibit C_k NOT quantum gates via Rydberg blockade, Quantum Inf. Process. **10**, 755 (2011).

[14] W.-X. Cui, S. Hu, H.-F. Wang, A.-D. Zhu, and S. Zhang, Scheme for implementing n-qubit controlled phase gate of photons assisted by quantum-dot-microcavity coupled system: optimal probability of success, Laser Phys. Lett. **12**, 055201 (2015).

[15] S. L. Su, Rydberg quantum controlled-phase gate with one control and multiple target qubits*, Chinese Phys. B **27**, 110304 (2018).

[16] D. E. Deutsch, Quantum computational networks, Proc. R. Soc. London A **425**, 73 (1989).

[17] X.-F. Shi, Deutsch, Toffoli, and cnot gates via Rydberg blockade of neutral atoms, Phys. Rev. Appl. **9**, 051001(R) (2018).

[18] X. Jiang, J. Scott, M. Friesen, and M. Saffman, Sensitivity of quantum gate fidelity to laser phase and intensity noise, Phys. Rev. A **107**, 042611 (2023).

[19] H. Bernien, S. Schwartz, A. Keesling, H. Levine, A. Omran, H. Pichler, S. Choi, A. S. Zibrov, M. Endres, M. Greiner, V. Vuletić, and M. D. Lukin, Probing many-body dynamics on a 51-atom quantum simulator, Nature (London) **551**, 579 (2017).

[20] A. Keesling, A. Omran, H. Levine, H. Bernien, H. Pichler, S. Choi, R. Samajdar, S. Schwartz, P. Silvi, S. Sachdev, P. Zoller, M. Endres, M. Greiner, V. Vuletić, and M. D. Lukin, Quantum Kibble–Zurek mechanism and critical dynamics on a programmable Rydberg simulator, Nature (London) **568**, 207 (2019).

[21] A. Omran, H. Levine, A. Keesling, G. Semeghini, T. T. Wang, S. Ebadi, H. Bernien, A. S. Zibrov, H. Pichler, S. Choi *et al.*, Generation and manipulation of Schrödinger cat states in Rydberg atom arrays, Science **365**, 570 (2019).

[22] D. Comparat and P. Pillet, Dipole blockade in a cold Rydberg atomic sample, J. Opt. Soc. Am. B **27**, A208 (2010).

[23] L. Béguin, A. Vernier, R. Chicireanu, T. Lahaye, and A. Browaeys, Direct measurement of the van der Waals interaction between two Rydberg atoms, Phys. Rev. Lett. **110**, 263201 (2013).

[24] M. Saffman, Quantum computing with atomic qubits and Rydberg interactions: progress and challenges, J. Phys. B: At. Mol. Opt. Phys. **49**, 202001 (2016).

[25] T. M. Graham, M. Kwon, B. Grinkemeyer, Z. Marra, X. Jiang, M. T. Lichtman, Y. Sun, M. Ebert, and M. Saffman, Rydberg-mediated entanglement in a two-dimensional neutral atom qubit array, Phys. Rev. Lett. **123**, 230501 (2019).

[26] D. Barredo, S. de Léséleuc, V. Lienhard, T. Lahaye, and A. Browaeys, An atom-by-atom assembler of defect-free arbitrary two-dimensional atomic arrays, Science **354**, 1021 (2016).

[27] H. J. Metcalf and P. van der Straten, Laser cooling and trapping of atoms, J. Opt. Soc. Am. B **20**, 887 (2003).

[28] M.-T. Nguyen, J.-G. Liu, J. Wurtz, M. D. Lukin, S.-T. Wang, and H. Pichler, Quantum optimization with arbitrary connectivity using Rydberg atom arrays, PRX Quantum **4**, 010316 (2023).

[29] K. Srakaew, P. Weckesser, S. Hollerith, D. Wei, D. Adler, I. Bloch, and J. Zeiher, A subwavelength atomic array switched by a single Rydberg atom, Nat. Phys. **19**, 714 (2023).

[30] S. Ebadi, A. Keesling, M. Cain, T. T. Wang, H. Levine, D. Bluvstein, G. Semeghini, A. Omran, J.-G. Liu, R. Samajdar,

X.-Z. Luo, B. Nash, X. Gao, B. Barak, E. Farhi, S. Sachdev, N. Gemelke, L. Zhou, S. Choi, H. Pichler *et al.*, Quantum optimization of maximum independent set using Rydberg atom arrays, Science **376**, 1209 (2022).

[31] G. K. Brennen, C. M. Caves, P. S. Jessen, and I. H. Deutsch, Quantum logic gates in optical lattices, Phys. Rev. Lett. **82**, 1060 (1999).

[32] G. K. Brennen, I. H. Deutsch, and P. S. Jessen, Entangling dipole-dipole interactions for quantum logic with neutral atoms, Phys. Rev. A **61**, 062309 (2000).

[33] D. S. Weiss and M. Saffman, Quantum computing with neutral atoms, Phys. Today **70**, 44 (2017).

[34] T. M. Graham, Y. Song, J. Scott, C. Poole, L. Phuttitarn, K. Jooya, P. Eichler, X. Jiang, A. Marra, B. Grinkemeyer, M. Kwon, M. Ebert, J. Cherek, M. T. Lichtman, M. Gillette, J. Gilbert, D. Bowman, T. Ballance, C. Campbell, E. D. Dahl *et al.*, Multi-qubit entanglement and algorithms on a neutral-atom quantum computer, Nature (London) **604**, 457 (2022).

[35] S. J. Evered, D. Bluvstein, M. Kalinowski, S. Ebadi, T. Manovitz, H. Zhou, S. H. Li, A. A. Geim, T. T. Wang, N. Maskara *et al.*, High-fidelity parallel entangling gates on a neutral atom quantum computer, Nature (London) **622**, 268 (2023).

[36] F. Wilczek and A. Zee, Appearance of gauge structure in simple dynamical systems, Phys. Rev. Lett. **52**, 2111 (1984).

[37] M. V. Berry, Quantal phase factors accompanying adiabatic changes, Proc. R. Soc. London A **392**, 45 (1984).

[38] Y. Aharonov and J. Anandan, Phase change during a cyclic quantum evolution, Phys. Rev. Lett. **58**, 1593 (1987).

[39] J. Pachos, P. Zanardi, and M. Rasetti, Non-Abelian Berry connections for quantum computation, Phys. Rev. A **61**, 010305(R) (1999).

[40] W. Xiang-Bin and M. Keiji, Nonadiabatic conditional geometric phase shift with NMR, Phys. Rev. Lett. **87**, 097901 (2001).

[41] S.-L. Zhu and Z. D. Wang, Implementation of universal quantum gates based on nonadiabatic geometric phases, Phys. Rev. Lett. **89**, 097902 (2002).

[42] J. T. Thomas, M. Lababidi, and M. Tian, Robustness of single-qubit geometric gate against systematic error, Phys. Rev. A **84**, 042335 (2011).

[43] P. Z. Zhao, X.-D. Cui, G. F. Xu, E. Sjöqvist, and D. M. Tong, Rydberg-atom-based scheme of nonadiabatic geometric quantum computation, Phys. Rev. A **96**, 052316 (2017).

[44] K. Z. Li, P. Z. Zhao, and D. M. Tong, Approach to realizing nonadiabatic geometric gates with prescribed evolution paths, Phys. Rev. Res. **2**, 023295 (2020).

[45] T. Chen and Z.-Y. Xue, Nonadiabatic geometric quantum computation with parametrically tunable coupling, Phys. Rev. Appl. **10**, 054051 (2018).

[46] C. Zhang, T. Chen, S. Li, X. Wang, and Z.-Y. Xue, High-fidelity geometric gate for silicon-based spin qubits, Phys. Rev. A **101**, 052302 (2020).

[47] B.-J. Liu, X.-K. Song, Z.-Y. Xue, X. Wang, and M.-H. Yung, Plug-and-play approach to nonadiabatic geometric quantum gates, Phys. Rev. Lett. **123**, 100501 (2019).

[48] E. Sjöqvist, D. M. Tong, L. M. Andersson, B. Hessmo, M. Johansson, and K. Singh, Non-adiabatic holonomic quantum computation, New J. Phys. **14**, 103035 (2012).

[49] G. F. Xu, J. Zhang, D. M. Tong, E. Sjöqvist, and L. C. Kwek, Nonadiabatic holonomic quantum computation in decoherence-free subspaces, Phys. Rev. Lett. **109**, 170501 (2012).

[50] Z.-Y. Xue, J. Zhou, and Z. D. Wang, Universal holonomic quantum gates in decoherence-free subspace on superconducting circuits, Phys. Rev. A **92**, 022320 (2015).

[51] Z.-Y. Xue, F.-L. Gu, Z.-P. Hong, Z.-H. Yang, D.-W. Zhang, Y. Hu, and J. Q. You, Nonadiabatic holonomic quantum computation with dressed-state qubits, Phys. Rev. Appl. **7**, 054022 (2017).

[52] J. Zhou, B. Liu, Z. Hong, and Z. Xue, Fast holonomic quantum computation based on solid-state spins with all-optical control, Sci. China Phys. Mech. Astron. **61**, 010312 (2018).

[53] Z.-P. Hong, B.-J. Liu, J.-Q. Cai, X.-D. Zhang, Y. Hu, Z. D. Wang, and Z.-Y. Xue, Implementing universal nonadiabatic holonomic quantum gates with transmons, Phys. Rev. A **97**, 022332 (2018).

[54] V. Azimi Mousolou, Electric nonadiabatic geometric entangling gates on spin qubits, Phys. Rev. A **96**, 012307 (2017).

[55] P. Z. Zhao, K. Z. Li, G. F. Xu, and D. M. Tong, General approach for constructing hamiltonians for nonadiabatic holonomic quantum computation, Phys. Rev. A **101**, 062306 (2020).

[56] M. Johansson, E. Sjöqvist, L. M. Andersson, M. Ericsson, B. Hessmo, K. Singh, and D. M. Tong, Robustness of nonadiabatic holonomic gates, Phys. Rev. A **86**, 062322 (2012).

[57] S.-B. Zheng, C.-P. Yang, and F. Nori, Comparison of the sensitivity to systematic errors between nonadiabatic non-Abelian geometric gates and their dynamical counterparts, Phys. Rev. A **93**, 032313 (2016).

[58] N. Ramberg and E. Sjöqvist, Environment-assisted holonomic quantum maps, Phys. Rev. Lett. **122**, 140501 (2019).

[59] J. Jing, C.-H. Lam, and L.-A. Wu, Non-Abelian holonomic transformation in the presence of classical noise, Phys. Rev. A **95**, 012334 (2017).

[60] J. Anandan, Non-adiabatic non-Abelian geometric phase, Phys. Lett. A **133**, 171 (1988).

[61] G. F. Xu, P. Z. Zhao, T. H. Xing, E. Sjöqvist, and D. M. Tong, Composite nonadiabatic holonomic quantum computation, Phys. Rev. A **95**, 032311 (2017).

[62] Z. Zhu, T. Chen, X. Yang, J. Bian, Z.-Y. Xue, and X. Peng, Single-loop and composite-loop realization of nonadiabatic holonomic quantum gates in a decoherence-free subspace, Phys. Rev. Appl. **12**, 024024 (2019).

[63] Y. Sekiguchi, Y. Komura, and H. Kosaka, Dynamical decoupling of a geometric qubit, Phys. Rev. Appl. **12**, 051001(R) (2019).

[64] X. Wu and P. Z. Zhao, Universal nonadiabatic geometric gates protected by dynamical decoupling, Phys. Rev. A **102**, 032627 (2020).

[65] T. Yan, B.-J. Liu, K. Xu, C. Song, S. Liu, Z. Zhang, H. Deng, Z. Yan, H. Rong, K. Huang, M.-H. Yung, Y. Chen, and D. Yu, Experimental realization of nonadiabatic shortcut to non-Abelian geometric gates, Phys. Rev. Lett. **122**, 080501 (2019).

[66] S. Li, T. Chen, and Z.-Y. Xue, Fast holonomic quantum computation on superconducting circuits with optimal control, Adv. Quantum Technol. **3**, 2000001 (2020).

[67] M.-Z. Ai, S. Li, Z. Hou, R. He, Z.-H. Qian, Z.-Y. Xue, J.-M. Cui, Y.-F. Huang, C.-F. Li, and G.-C. Guo, Experimental realization of nonadiabatic holonomic single-qubit quantum

gates with optimal control in a trapped ion, Phys. Rev. Appl. **14**, 054062 (2020).
[68] S. Li and Z.-Y. Xue, Dynamically corrected nonadiabatic holonomic quantum gates, Phys. Rev. Appl. **16**, 044005 (2021).
[69] G. F. Xu, D. M. Tong, and E. Sjöqvist, Path-shortening realizations of nonadiabatic holonomic gates, Phys. Rev. A **98**, 052315 (2018).
[70] F. Zhang, J. Zhang, P. Gao, and G. Long, Searching nonadiabatic holonomic quantum gates via an optimization algorithm, Phys. Rev. A **100**, 012329 (2019).
[71] T. Chen, P. Shen, and Z.-Y. Xue, Robust and fast holonomic quantum gates with encoding on superconducting circuits, Phys. Rev. Appl. **14**, 034038 (2020).
[72] B.-J. Liu, Z.-Y. Xue, and M.-H. Yung, Brachistochrone non-Adiabatic holonomic quantum control, arXiv:2001.05182.
[73] Z. Han, Y. Dong, B. Liu, X. Yang, S. Song, L. Qiu, D. Li, J. Chu, W. Zheng, J. Xu, T. Huang, Z. Wang, X. Yu, X. Tan, D. Lan, M.-H. Yung, and Y. Yu, Experimental realization of universal time-optimal non-Abelian geometric gates, arXiv:2004.10364.
[74] P. Zhao, Z. Dong, Z. Zhang, G. Guo, D. Tong, and Y. Yin, Experimental realization of nonadiabatic geometric gates with a superconducting xmon qubit, Sci. China Phys. Mech. Astron. **64**, 250362 (2021).
[75] A. A. Abdumalikov Jr., J. M. Fink, K. Juliusson, M. Pechal, S. Berger, A. Wallraff, and S. Filipp, Experimental realization of non-Abelian non-adiabatic geometric gates, Nature (London) **496**, 482 (2013).
[76] C. Song, S.-B. Zheng, P. Zhang, K. Xu, L. Zhang, Q. Guo, W. Liu, D. Xu, H. Deng, K. Huang, D. Zheng, X. Zhu, and H. Wang, Continuous-variable geometric phase and its manipulation for quantum computation in a superconducting circuit, Nat. Commun. **8**, 1061 (2017).
[77] L. Qiu, H. Li, Z. Han, W. Zheng, X. Yang, Y. Dong, S. Song, D. Lan, X. Tan, and Y. Yu, Experimental realization of noncyclic geometric gates with shortcut to adiabaticity in a superconducting circuit, Appl. Phys. Lett. **118**, 254002 (2021).
[78] C. Zu, W.-B. Wang, L. He, W.-G. Zhang, C.-Y. Dai, F. Wang, and L.-M. Duan, Experimental realization of universal geometric quantum gates with solid-state spins, Nature (London) **514**, 72 (2014).
[79] Y. Sekiguchi, N. Niikura, R. Kuroiwa, H. Kano, and H. Kosaka, Optical holonomic single quantum gates with a geometric spin under a zero field, Nat. Photon **11**, 309 (2017).
[80] B. B. Zhou, P. C. Jerger, V. O. Shkolnikov, F. J. Heremans, G. Burkard, and D. D. Awschalom, Holonomic quantum control by coherent optical excitation in diamond, Phys. Rev. Lett. **119**, 140503 (2017).
[81] G. Feng, G. Xu, and G. Long, Experimental realization of nonadiabatic holonomic quantum computation, Phys. Rev. Lett. **110**, 190501 (2013).
[82] H. Li, Y. Liu, and G. Long, Experimental realization of single-shot nonadiabatic holonomic gates in nuclear spins, Sci. China Phys. Mech. Astron. **60**, 080311 (2017).
[83] K. Khodjasteh and L. Viola, Dynamically error-corrected gates for universal quantum computation, Phys. Rev. Lett. **102**, 080501 (2009).
[84] X. Wang, L. S. Bishop, J. P. Kestner, E. Barnes, K. Sun, and S. Das Sarma, Composite pulses for robust universal control of singlet–triplet qubits, Nat. Commun. **3**, 997 (2012).
[85] X. Rong, J. Geng, F. Shi, Y. Liu, K. Xu, W. Ma, F. Kong, Z. Jiang, Y. Wu, and J. Du, Experimental fault-tolerant universal quantum gates with solid-state spins under ambient conditions, Nat. Commun. **6**, 8748 (2015).
[86] B.-J. Liu, Y.-S. Wang, and M.-H. Yung, Super-robust nonadiabatic geometric quantum control, Phys. Rev. Res. **3**, L032066 (2021).
[87] T. Sleator and H. Weinfurter, Realizable universal quantum logic gates, Phys. Rev. Lett. **74**, 4087 (1995).
[88] J. T. Young, P. Bienias, R. Belyansky, A. M. Kaufman, and A. V. Gorshkov, Asymmetric blockade and multiqubit gates via dipole-dipole interactions, Phys. Rev. Lett. **127**, 120501 (2021).
[89] K. M. Maller, M. T. Lichtman, T. Xia, Y. Sun, M. J. Piotrowicz, A. W. Carr, L. Isenhower, and M. Saffman, Rydberg-blockade controlled-NOT gate and entanglement in a two-dimensional array of neutral-atom qubits, Phys. Rev. A **92**, 022336 (2015).
[90] X.-F. Shi, F. Bariani, and T. A. B. Kennedy, Entanglement of neutral-atom chains by spin-exchange Rydberg interaction, Phys. Rev. A **90**, 062327 (2014).
[91] C.-J. Lorenzen and K. Niemax, Precise quantum defects of nS, nP and nD levels in cS I, Z. Phys. A **315**, 127 (1984).
[92] K.-H. Weber and C. J. Sansonetti, Accurate energies of nS, nP, nD, nF, and nG levels of neutral cesium, Phys. Rev. A **35**, 4650 (1987).
[93] I. I. Beterov, I. I. Ryabtsev, D. B. Tretyakov, and V. M. Entin, Quasiclassical calculations of blackbody-radiation-induced depopulation rates and effective lifetimes of Rydberg nS, nP, and nD alkali-metal atoms with $n \leqslant 80$, Phys. Rev. A **79**, 052504 (2009).
[94] M. A. Nielsen, A simple formula for the average gate fidelity of a quantum dynamical operation, Phys. Lett. A **303**, 249 (2002).
[95] A. G. White, A. Gilchrist, G. J. Pryde, J. L. O'Brien, M. J. Bremner, and N. K. Langford, Measuring two-qubit gates, J. Opt. Soc. Am. B **24**, 172 (2007).
[96] Y. Shapira, R. Shaniv, T. Manovitz, N. Akerman, and R. Ozeri, Robust entanglement gates for trapped-ion qubits, Phys. Rev. Lett. **121**, 180502 (2018).
[97] X.-F. Shi, Fast, accurate, and realizable two-qubit entangling gates by quantum interference in detuned rabi cycles of Rydberg atoms, Phys. Rev. Appl. **11**, 044035 (2019).
[98] I. I. Ryabtsev, I. I. Beterov, D. B. Tretyakov, V. M. Entin, and E. A. Yakshina, Doppler- and recoil-free laser excitation of Rydberg states via three-photon transitions, Phys. Rev. A **84**, 053409 (2011).
[99] X.-F. Shi, Suppressing motional dephasing of ground-rydberg transition for high-fidelity quantum control with neutral atoms, Phys. Rev. Appl. **13**, 024008 (2020).
[100] A. M. Kaufman, B. J. Lester, and C. A. Regal, Cooling a single atom in an optical tweezer to its quantum ground state, Phys. Rev. X **2**, 041014 (2012).
[101] A. Reiserer, C. Nölleke, S. Ritter, and G. Rempe, Ground-state cooling of a single atom at the center of an optical cavity, Phys. Rev. Lett. **110**, 223003 (2013).
[102] Y. Zeng, P. Xu, X. He, Y. Liu, M. Liu, J. Wang, D. J. Papoular, G. V. Shlyapnikov, and M. Zhan, Entangling two individual atoms of different isotopes via Rydberg blockade, Phys. Rev. Lett. **119**, 160502 (2017).

[103] C. J. Picken, R. Legaie, K. McDonnell, and J. D. Pritchard, Entanglement of neutral-atom qubits with long ground-rydberg coherence times, Quantum Sci. Technol. **4**, 015011 (2018).

[104] J.-L. Wu, S.-L. Su, Y. Wang, J. Song, Y. Xia, and Y.-Y. Jiang, Effective Rabi dynamics of Rydberg atoms and robust high-fidelity quantum gates with a resonant amplitude-modulation field, Opt. Lett. **45**, 1200 (2020).

[105] H. Levine, A. Keesling, G. Semeghini, A. Omran, T. T. Wang, S. Ebadi, H. Bernien, M. Greiner, V. Vuletić, H. Pichler, and M. D. Lukin, Parallel implementation of high-fidelity multiqubit gates with neutral atoms, Phys. Rev. Lett. **123**, 170503 (2019).

[106] M. Ebert, M. Kwon, T. G. Walker, and M. Saffman, Coherence and Rydberg blockade of atomic ensemble qubits, Phys. Rev. Lett. **115**, 093601 (2015).

[107] A. W. Glaetzle, R. M. W. van Bijnen, P. Zoller, and W. Lechner, A coherent quantum annealer with Rydberg atoms, Nat. Commun. **8**, 15813 (2017).

[108] C. P. Williams and C. Bennett, Explorations in quantum computing, Phys. Today **52**, 66 (1999).